iScience

Article

Release of extracellular DNA by *Pseudomonas* sp. as a major determinant for biofilm switching and an early indicator for cell population control

Graphical abstract

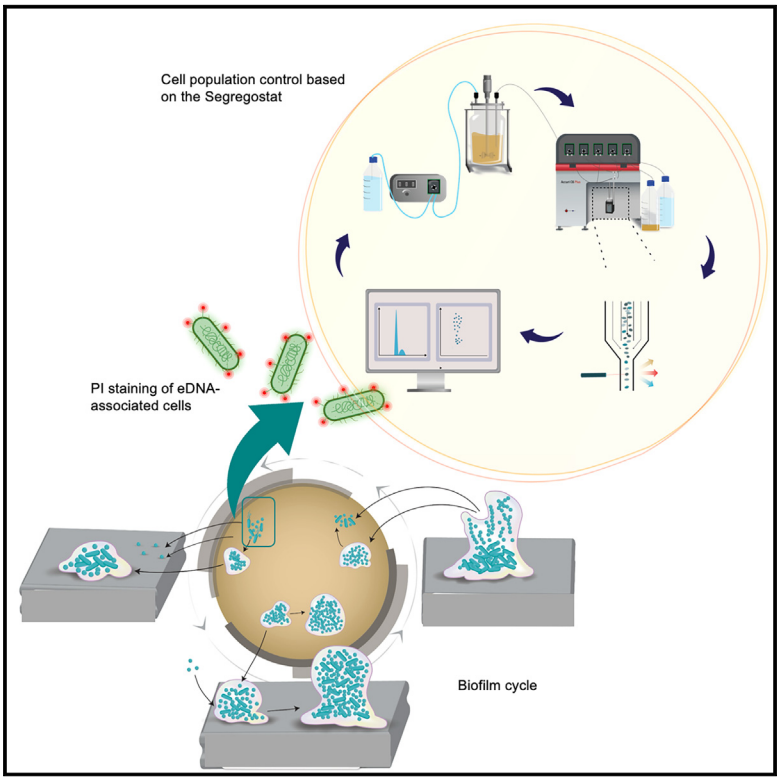

Authors

Fatemeh Bajoul Kakahi, Juan Andres Martinez, Fabian Moreno Avitia, Daniel C. Volke, Nicolas T. Wirth, Pablo I. Nikel, Frank Delvigne

Correspondence

f.delvigne@uliege.be

In brief

Biological sciences; Microbiology; Microbiofilms

Highlights

- Cells associated with eDNA can be detected early in the planktonic phase
- The number of eDNA-associated cells correlates with global biofilm formation
- Automated FC of eDNA-associated cells allow probing biofilm switching
- Automated glucose pulsing mitigates biofilm formation

Kakahi et al., 2025, iScience *28*, 112063
March 21, 2025
https://doi.org/10.1016/j.isci.2025.112063

CellPress

iScience

CellPress
OPEN ACCESS

Article

Release of extracellular DNA by *Pseudomonas* sp. as a major determinant for biofilm switching and an early indicator for cell population control

Fatemeh Bajoul Kakahi,[1] Juan Andres Martinez,[1] Fabian Moreno Avitia,[1] Daniel C. Volke,[2] Nicolas T. Wirth,[2] Pablo I. Nikel,[2] and Frank Delvigne[1,3,*]

[1]Terra Research and Teaching Centre, Micro Bial Processes and Interactions (MiPI), Gembloux Agro-Bio Tech, University of Liege, Gembloux, Belgium

[2]The Novo Nordisk Foundation Center for Biosustainability, Technical University of Denmark, Kongens Lyngby 2800, Denmark

[3]Lead contact

*Correspondence: f.delvigne@uliege.be

https://doi.org/10.1016/j.isci.2025.112063

SUMMARY

In *Pseudomonas* sp., the switch from planktonic to sessile state is driven by extracellular DNA release. We observed a subpopulation of cells associated with eDNA in the planktonic phase, as indicated by propidium iodide staining. Surprisingly, the size of this subpopulation was directly correlated with the overall biofilm-forming capacity of the population. This challenges the prevailing understanding of phenotypic switching and confirms that biofilm formation in *Pseudomonas* is a collective process governed by eDNA release. Automated flow cytometry tracked the process, and PI-positive cells were identified as an early indicator of biofilm formation. Automated glucose pulsing successfully reduced biofilm formation by interfering with PI-positive cell proliferation. This study provides insights into the collective determinants of biofilm switching in *Pseudomonas putida* and introduces a potential strategy for controlling biofilm formation.

INTRODUCTION

The transition from a planktonic to a biofilm state in a bacterial population can be influenced by a variety of factors and is a complex process that can vary depending on the microbial species considered and the environmental conditions.[1–3] However, this transition has been poorly investigated so far due to the lack of single cell proxies related to biofilm switching. It has been previously suggested that a subpopulation of cells within a planktonic culture may play a role in initiating biofilm formation by binding to extracellular DNA (eDNA).[4] These cells can further serve as pioneers that start the biofilm formation process by adhering to surfaces and facilitating the recruitment of other cells to form either a mono- or a multi-species biofilm. In this context, it has been recently suggested that the process of cell aggregation in the liquid phase is a critical step in the biofilm life cycle.[5,6] These aggregates offer several advantages over individual planktonic cells, including increased antibiotic resistance and improved surface colonization.[6–8] Bacterial aggregation is influenced by various factors, such as quorum sensing, eDNA, ions, and cationic polymers.[9–12] Collectively, previous studies reveal that bacteria exhibit complex multicellular behaviors in planktonic phase that differ fundamentally from those observed in surface-attached biofilms. This distinction highlights the importance of considering cell auto-aggregation (i.e., aggregation between cells of the same species) and co-aggregation (i.e., aggregation between cells of different species) as crucial components of the biofilm cycle model, necessitating a revision of the current understanding of biofilm development and dynamics.[3]

The involvement of eDNA in the formation of bacterial aggregates has been observed in various bacterial species.[13–16] eDNA plays multiple roles within the aggregate, serving as a structural component, as an energy and nutrition source, and as a gene pool for horizontal gene transfer in naturally competent bacteria.[17,18] Additionally, eDNA can bind to bacterial flagella, leading to increased hydrophobicity of the cell surface. This, in turn, promotes bacterial aggregation and enhances the stability of the biofilm structure.[19–21] *Pseudomonas putida* KT2440 is a non-pathogenic soil bacterium endowed with the ability to adapt to a large variety of physicochemical and nutritional niches,[22,23] and able to form biofilms depending on the environmental conditions.[24] *P. putida* has been a laboratory model for examining the lifestyle and activities of environmental bacteria.[25] Accumulating evidence on attachment and biofilm formation by *P. putida* offers a detailed perspective of the functional steps involved in the process and the regulatory networks.[26] Current research indicates that the second messenger, cyclic diguanosine-5′-monophosphate (c-di-GMP), plays a global role in regulating the transition between motile and sessile lifestyles in *P. putida*.[26,27] However, the regulatory network controlling c-di-GMP[25] is complex and not fully described yet. Additionally, the current information indicates that in, *P. putida*, adhesins (primarily LapA but also LapF) are the key components for

attachment and biofilm buildup, and EPS mainly functions as a protective barrier for the sessile population against external stress factors. A structural and regulatory interplay between adhesins and EPS has been assumed,[28–30] but it lacks detailed investigation. Therefore, many researchers have focused on either an indirect method for c-di-GMP measurement or developing a fluorescence-based biosensor based on translational fusion with LapA or LapF.[27] Although substantial advancements have been achieved in characterizing the various stages of biofilm development, the current knowledge primarily concentrates on studying mature biofilms or examining differential gene expression during the transition from planktonic to biofilm states.[26,27] Nevertheless, due to the complexity of the regulatory network governing biofilm formation in *P. putida*, relying on a robust single-cell proxy to describe the initial steps for biofilm production is challenging.

In our work, by using *P. putida* KT2440 and derivatives exhibiting either enhanced or reduced biofilm formation capabilities, we observed a fraction of cells associated with eDNA in the planktonic phase. This observation was based on propidium iodide (PI) staining. More importantly, it was determined that the size of the fraction of eDNA-associated/PI-positive cells is correlated to the global biofilm formation capability of the cell population. This result is important since it suggests that biofilm switching does not follow the classical phenotypic switching mechanism where individual cells within the population decide to activate or repress gene circuits according to environmental cues.[31–33] The same observation has been previously reported for *P. aeruginosa* for which massive release of eDNA increases the probability of binding to cells and the number of eDNA-associated cells, in turn, increases the probability of cell aggregation and biofilm formation. Accordingly, biofilm switching in *Pseudomonas* species is determined collectively based on the number of eDNA molecules released in the supernatant.[17] More specifically, this study showed that eDNA release events determine where and when *P. aeruginosa* cells begin to aggregate to subsequently form biofilms and that the number of eDNA-associated cells correlates with increased numbers of cell aggregates and the size of the mature biofilm. In this work, we will use these characteristics to characterize the dynamics of *P. putida* population upon continuous cultivation based on automated flow cytometry (FC).[34] In a second step, reactive FC strategies[35,36] will be implemented for acting on the cell phenotypic switching mechanisms associated with biofilm formation to either reduce or enhance biofilm formation.

RESULTS

PI staining is an efficient approach for detecting eDNA-associated cells in *Pseudomonas* sp. populations

Previous studies have shown that propidium iodide (PI) can bind to eDNA and produce a red-but-not-dead signal.[4,37–39] Since eDNA is an important component involved in biofilm formation, we decided to investigate the potential use of PI as a single-cell proxy for identifying subpopulations involved in the transition to biofilm. We used *P. putida* DGC, a derivative of *P. putida* KT2440 overproducing c-di-GMP, leading to increased biofilm formation capability. *P. putida* DGC was cultivated in a shake flask for 24h, and samples were collected after 6h (exponential phase), 12h (late exponential phase), and 24h (stationary phase) (Figure 1A). Cell samples were then double-stained with PI and SYTO9 and observed with high resolution confocal laser scanning microscopy (CLSM). Using this staining method, dead cells exhibit bright red fluorescence upon PI binding to intracellular DNA, quenching the green fluorescence associated with SYTO9 (Figure 1B). In contrast, live cells remain green due to SYTO9, as PI cannot penetrate intact membranes (Figure 1B). Notably, our analysis revealed a significant proportion of ''intermediate'' phenotypes (Figure 1C), characterized by green fluorescent cells displaying irregular red dots at their surface. These PI patches correspond to eDNA fragments attached to the cell surface. Since PI is external to the cell, the green fluorescence associated with SYTO9 remains unaffected. External PI staining is particularly visible in cell aggregates (Figure 1D). FC analyses pointed out this PI-positive, eDNA-associated, subpopulation was generated very early during the cultivation, with a PI signal lower than the one recorded for dead cells (Figure 1E). To assess the viability of these subpopulations, we performed Redox Sensor Green (RSG) staining, an indicator of metabolic activity (Figure 1F).[40] This dye becomes fluorescent when reduced by cellular reductases. Our data demonstrated that both strains exhibited high metabolic activity at all sampling points during cultivation (Figure S2). These results indicated these cells were not dead but rather metabolically active (Figure 1F). Similar experiments were also performed based on the wild-type strain *P. putida* KT2440 (Figure S2). We further treated the biofilm samples with DNAse (Figure 1G). For all the samples, we observed a significant decrease in the number of PI-positive cells, suggesting that PI staining is due to the association of cells with eDNA.

Finally, the analysis of the biofilm phase using FC revealed that most of the cells (91%) were PI-positive (Figure 1G). We also processed the samples with DNAse and observed again a significant decrease (33%) in the PI-positive subpopulation following treatment with DNase enzyme (Figure 1H). These DNase-treated biofilm samples were also visualized using CLSM (Figure 1H). The results clearly demonstrated that PI signals were much more intense in the non-treated sample compared to the sample treated with DNase (Figure 1G). Subsequently, we employed CLSM to visualize the distribution of eDNA in the aggregation and biofilm samples, using the SYTO60 stain for bacterial cells and the TOTO-1 stain for eDNA. It has been reported that TOTO-1 for eDNA, combined with SYTO60 as a counterstain, can produce high-quality images of eDNA in various Gram-negative and Gram-positive bacterial species.[41] The obtained images clearly showed a substantial amount of eDNA in both types of samples (Figures S3B and S3D). We also observed a higher percentage of the PI-positive fraction in biofilm and aggregate samples, which could be attributed to the association between eDNA and PI.

Biofilm switching is determined early in the planktonic phase by a subpopulation of eDNA-associated cells

We first investigated biofilm switching based on standard cultivations in shake flasks. To establish a possible link between early eDNA excretion, PI staining and biofilm formation, we used different strains of *P. putida* exhibiting different biofilm forming

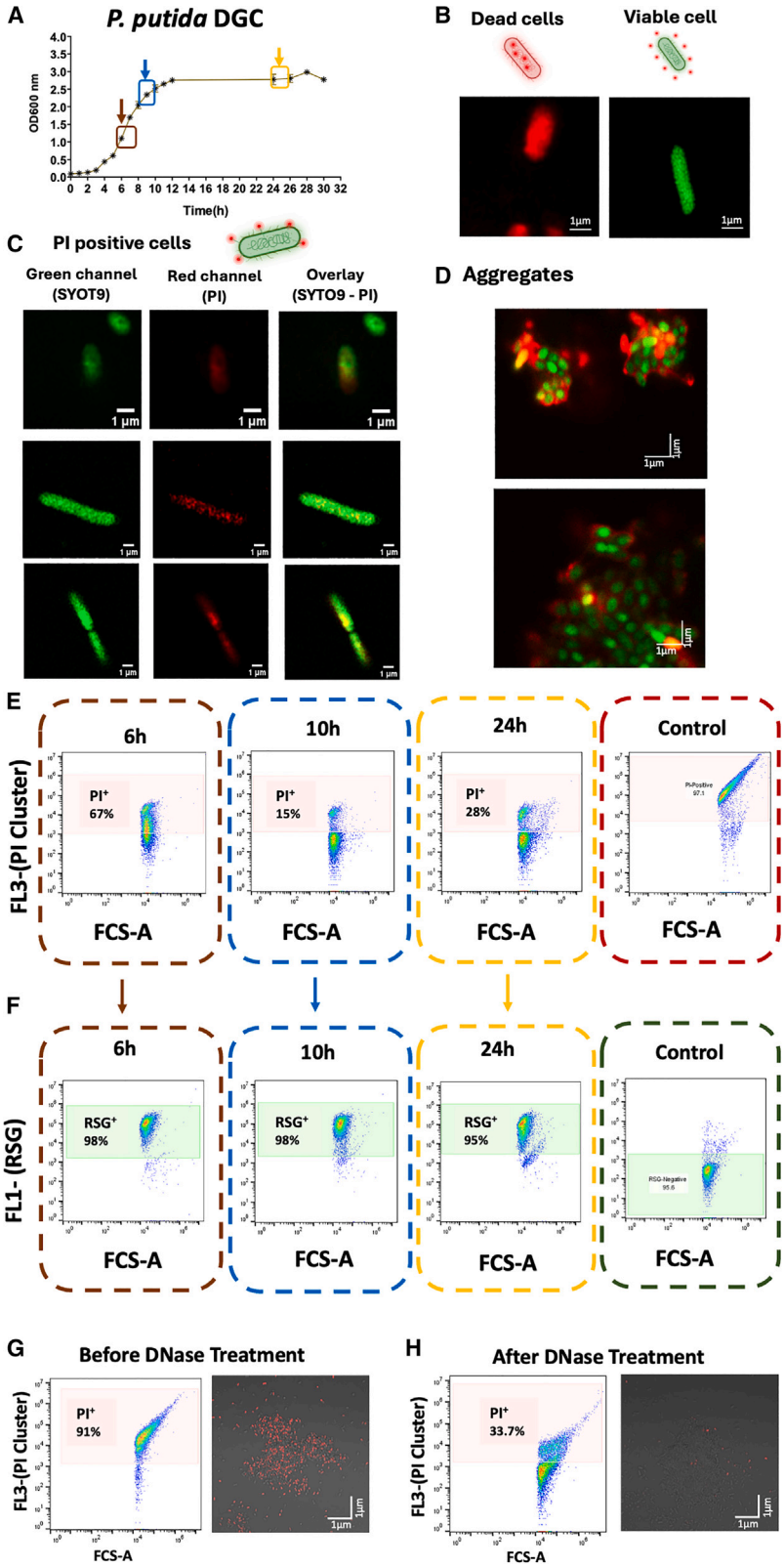

Figure 1. Occurrence of viable, PI-positive, cells in the planktonic phase during growth in shake flask

(A) Growth curves of *P. putida* DGC during 24h of batch cultivation were determined by spectrophotometric measurements (OD600), $n \geq 3$, the data are presented as mean ± standard deviation for three independent experiments.

(B) High resolution fluorescence microscopy (Airyscan) of *P. putida* DGC planktonic dead (heat treated) and live cells stained with a combination PI/SYTO9 (Scale bar: 1 μ m).

(C) High resolution fluorescence microscopy of *P. putida* DGC planktonic cells collected after 6h upon shake flask cultivation (state of the population displayed in panel E) and exhibiting partial PI staining (Scale bar: 1 μm. Three individual cells are shown. Additional cells have been analyzed and the pictures can be found in Figure S1).

(D) High resolution fluorescence microscopy of *P. putida* DGC cells in aggregates. Five individual fields of view per replicate and three biological replicates (Scale bar: 1 μ m).

(E) FC analyses of cell population based on PI staining ($n \geq 3$ independent experiments) (F) FC analyses of cell population for determining metabolic activity (RSG staining) at 6h, 10h, and 24h ($n \geq 3$ independent experiments).

(G and H) Effects of DNase treatment on PI positive fraction of biofilm sample. Sample showing significantly different PI uptake, before and after being treated by the DNase enzyme. Confocal laser scanning microscopy (CSLM) images of biofilm cells stained with PI before (G) and after (H) being treated with DNase enzyme. The red signal of the PI-positive fraction decreases significantly after DNase treatment (each flow cytometry analysis has been performed on $n = 3$ independent experiments. Statistics were performed using a One-way ANOVA test.

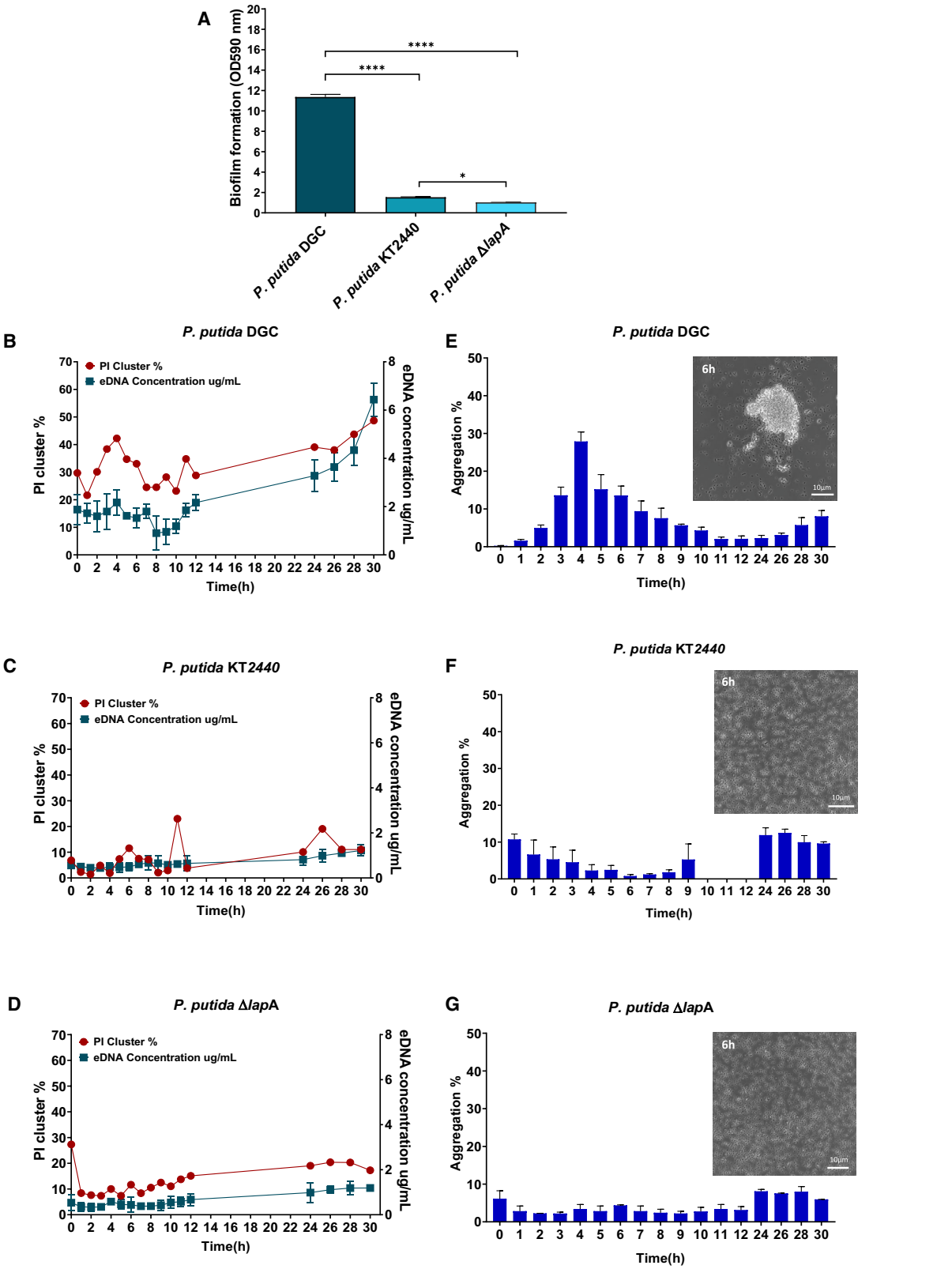

(legend on next page)

capabilities (Figure 2A). For this purpose, we genetically manipulated the bacteria by either reducing or increasing their biofilm-forming ability. Specifically, we knocked out the *lapA* gene, which encodes an adhesin involved in cell attachment, resulting in a strain that is unable to attach to abiotic surfaces. This Δ*lap*A derivative exhibits significantly reduced biofilm formation. On the other hand, to increase biofilm formation, we transformed *P. putida* with plasmid pS638DGC-244, generating a DGC strain (di-guanylate cyclase). This strain contains a more active di-guanylate cyclase that elevates the internal concentration of cyclic-di-GMP, a critical regulator of biofilm formation. High levels of c-di-GMP (c-di-GMP), support an adhesive lifestyle, while low levels lead to a planktonic lifestyle.[42] As expected, the *P. putida* DGC strain, with increased capacity for c-di-GMP production, exhibited the highest biofilm formation capability. On the contrary, the wild-type strain *P. putida* KT2440 exhibited low biofilm forming capability, which was further decreased upon the deletion of *lapA*. These *P. putida* strains (KT2440 and derivatives) were then cultivated in shake flask and monitored for PI staining and eDNA release (Figures 2B–2D). For all the strains, we observed a progressive accumulation of eDNA in the extracellular medium, correlated with the presence of PI-stained cells in the population. For the *P. putida* DGC strain, this effect was further increased, and cell aggregates were also observed during the cultivation. As a control experiment, the empty plasmid pS638 was transferred to the wild-type strains *P. putida* KT2440 and *P. putida* Δ*lap*A (Figure S4).

To assess the dynamic of auto-aggregation of *P. putida* KT2440, *P. putida* Δ*lap*A, and *P. putida* DGC during the shake flask cultivation, samples were analyzed by FC (Figures 2E–2G). Gating of the aggregated cells was done based on FSC and SSC signals. Interestingly, we observed an increase in aggregation during the beginning of the exponential growth phase, followed by a subsequent decrease upon entering the stationary phase, coinciding with the formation of the biofilm in the case of *P. putida* DGC (Figure 2E). However, this phenomenon was scarcely observed in the case of *P. putida* Δ*lap*A, which exhibited very low levels of cell aggregation (Figure 2F). On the other hand, *P. putida* KT2440 exhibited a more pronounced formation of aggregates compared to *P. putida* Δ*lap*A (Figure 2G). Furthermore, we conducted microscopy imaging on samples that were taken at the 6-h batch phase. The obtained images providing further evidence of pronounced aggregation occurring specifically in the case of *P. putida* DGC (Figures 2E–2G). The result indicates that the biofilm-forming capability of strains used in this study is highly related to auto-aggregation ability. A strong auto-aggregation was observed in *P. putida* DGC, which produces significantly higher biofilm compared to other tested strains (Figure S5). The presence of such aggregates is informative about a possible transition to biofilm lifestyle. Taken altogether, these data suggest that it could be possible to use PI as a molecular probe for tracking cells in planktonic phase in an early decision-making process for biofilm formation.

eDNA binding is correlated with cell auto-aggregation under dynamic cultivation conditions

We used automated FC for mapping the population diversification dynamics in continuous culture. For this purpose, we use an in-house developed FC interface for sampling a chemostat at the time interval of 12 min[39](Figure 3A). In this way, we obtained a high-resolution temporal profile of the evolution of the population based on three parameters i.e., the red fluorescence associated with PI binding (FL3-A channel), as well as the size and morphology of the cells and cell aggregates (FSC-A and SSC-A parameters respectively). Consistent with previous research, we observed that the transition to the biofilm lifestyle in *Pseudomonas* was promoted by the formation of cellular aggregates in the planktonic phase (Figure S5). We then applied a specific data treatment procedure to the temporal profile obtained based on the three signals obtained based on automated FC i.e., PI (Figure 3B), FSC (Figure 3C), and SSC (Figure 3D). We analyzed the population dynamics based on these three cellular features by dividing the scales attributed to each signal into 50 bins, each bin containing a specific number of cells. By comparing the number of cells in each bin during different time-point, a dynamic perspective can be obtained. We then computed the fluxes of cells into the phenotypic space by applying a gradient, leading to the quantification of the total fluxes of cells per time interval (F) for each signal (Figures 3E–3G). The observation of the time evolution of the flux of cells through the diversification landscape reveals useful information i.e., that flux of diversification occurs stochastically during chemostat cultivation (Figure 3H). Interestingly, data analysis pointed out a direct relationship between the FC signals (Figure 3I), suggesting a close interplay between the PI signal and cell auto-aggregation, and subsequent biofilm formation. This observation is in line with the dynamics of biofilm formation previously reported in the literature for other *Pseudomonas* strains, further validating the relevance of our automated FC protocol.

Biofilm formation is associated with a bursty diversification dynamics

In microbial ecology, phenotypic switching is often associated with a switching cost i.e., a loss of growth rate upon the activation of the alternative phenotype.[31,32] We recently demonstrated that this cost is the main driver for diversification dynamics of the

Figure 2. eDNA release increases the fraction of eDNA-associated cells in the planktonic phase

(A) Cristal violet assay for the biofilm forming capability of different derivatives of *P. putida* KT2440. Asterisks over brackets indicate a significant difference between samples (*p*-values: ****$p < 0.0001$, *$p < 0.03$). Results are presented as mean ± standard deviation. for three biological replicates. *N=3* independent experiments. Statistics were performed using a One-way ANOVA test.

(B–D) Time evolution of eDNA and PI-positive cells (determined based on FC) during flask experiments (experiments have been done in triplicates (3 independent experiments).

(E–G) Analysis of the auto-aggregation ability of E. *P. putida* DGC, F. *P. putida* KT2440, and G. *P. putida* Δ*lap*A, by flow cytometry ($n \geq 3$ independent experiments). The error bars represent the standard deviation (SD) for three biological replicates. Microscopy images (40×) of cell samples from flask experiments and three individual fields of view per replicate for E. *P. putida* DGC, F. *P. putida* KT2440, and G. *P. putida* Δ*lap*A after 6h of batch cultivation (n images ≥10, Figure S4) from $n = 3$ independent experiments (Scale bar: 10 μm).

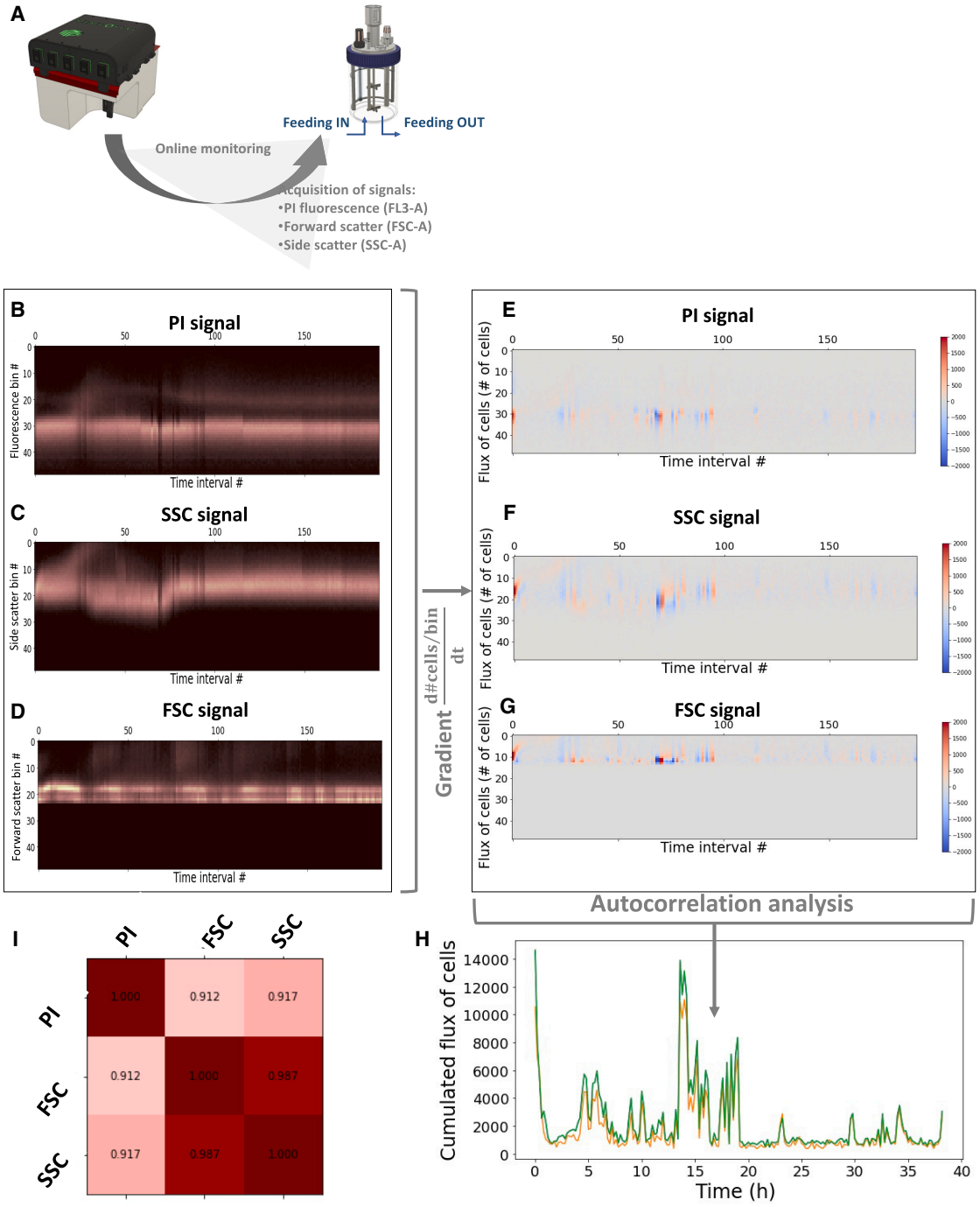

Figure 3. Automated FC analyses reveal a strong correlation between eDNA-associated, PI-positive cells and cell auto-aggregation

(A) Scheme of the automated FC set up connected to a continuous cultivation device (Dilution rate D = 0.1 h^{-1}).

(B–D) Binning of the time scatter profiles for the PI fluorescence, the FSC and SSC signals respectively (one time interval corresponds to 12 min).

(E–G) computation of the gradient of cells from the binned data for the PI fluorescence, the FSC and SSC signals respectively (one time interval corresponds to 12 min).

(H) Cumulated flux of cells extracted from the gradients of the three signals.

(I) Correlation matrix with the Pearson coefficients indicating a strong direct relationship between the FC signals (p-values $<10^{-78}$ for all the correlations).

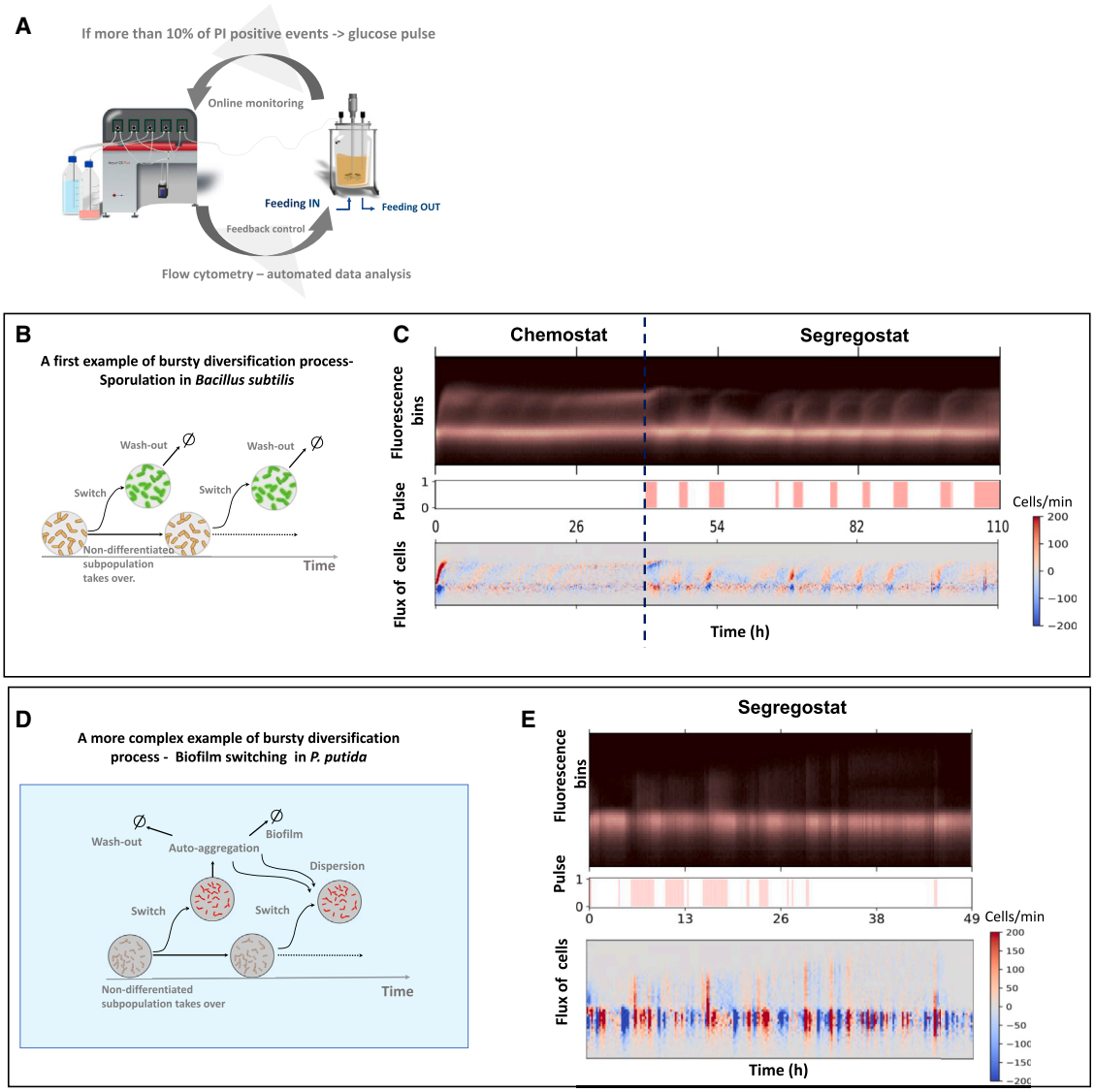

Figure 4. Biofilm switching in *P. putida* occurs based on a bursty diversification regime

(A) Scheme of the Segregostat. Pulses of nutrients are added in the function of the ratio between PI negative and PI positive cells (here set at 10% of PI positive cells), as recorded by automated FC.

(B) Example of bursty diversification process involved in the sporulation of *Bacillus subtilis*.

(C) By applying environmental forcing based on Segregostat cultivation, the number of bursts is reduced, and the fluxes of cells involved in the process are increased, leading to a substantial but temporary reduction of the entropy for the population (adapted form Henrion et al. 2023).[34](D) A more complex bursty diversification model proposed for *P. putida* KT2440.

(E) Time evolution of fluorescence bins associated with PI staining. Flux of cells into the phenotypic space is computed by applying a gradient to the binned data. Time evolution of the total flux of cells into phenotypic space (The fluxes of cells in the phenotypic space F(t) have been computed from the binned fluorescence data).

whole population.[34] To illustrate this concept, we will take one of our previously characterized cellular system as an example. In the case of the phenotypic switching associated with sporulation in *Bacillus subtilis*, it is obvious that spore formation leads to a drastic reduction in growth for the cell deciding to switch. In this case, since the switching cost associated with phenotypic switching is very high, a bursty diversification regime is observed. This regime is characterized by the appearance of spontaneous flux of cells (called bursts) phenotypically switching, these cells being progressively washed-out from the continuous cultivation device due to the loss of growth associated with the switching cost. This specific diversification regime was previously reported during cultivation performed in a device called Segregostat.[34] In short, the Segregostat cultivation protocol relies on the use of reactive FC (Figure 4A) to detect the bursts of diversification (in a way like the one used for the determination of

the fluxes of cells shown in (Figure 3E). When a burst of diversification is detected, a pulse of glucose is added to interfere with the natural diversification process i.e., by giving a growth advantage to the cells that are not differentiating. This concept is illustrated in the case of the sporulation in *Bacillus subtilis* (Figure 4B).[34] In this case, a P_{spoIIE}:GFP transcriptional reporter was used in order to detect the cells deciding to trigger sporulation. The bursts of cells can be visualized from the binned time scatter profile, as well as the concomitant fluxes of cells (Figure 4C). The observations made in the previous section point out that burstiness could also be associated with biofilm switching for *P. putida*. From a biological perspective, this would make sense since switching to the biofilm state, including cell auto-aggregation, results in a significant cost for the global growth of the population remaining in the liquid phase (Figures S6 and S7). However, a more complex diversification process must be expected since population dynamics can also be impacted by cell auto-aggregation and cell release from biofilm (Figure 4D). The diversification profile of *P. putida* associated with biofilm switching was then determined based on Segregostat cultivation and PI staining, according to an automated protocol for PI staining previously established for different Gram-negative bacteria, including *P. putida*.[39] As expected, bursts of diversification were also observed in this case (Figure 4E). While the amplitude of these bursts is reduced compared to the ones observed upon standard chemostat cultivation (Figure 3J), they are more frequent and follow approximately the same periodicity as for the glucose pulses. In the next section, the detection of these bursts will be considered as an early-warning indicator of biofilm switching for *P. putida* KT2440. The Segregostat system will then be used to interfere with these bursts of diversification and to mitigate biofilm formation.

Control of bursts leads to reduced population diversification and biofilm formation

In the previous section, we observed that the diversification dynamics associated with biofilm switching was bursty. Our previous experiences with other bursty systems, like the sporulation in *Bacillus subtilis* or the burdensome T7-based expression system in *E. coli*, pointed out that these systems can be easily perturbed based on glucose pulsing since the differentiated fraction of cells exhibits a significantly reduced growth rate by comparison with the non-differentiated one.[34] This approach seems also to hold in the case of biofilm switching, given the switching cost observed at this level (Figures S6 and S7). For this purpose, the diversification bursts were detected based on automated FC and glucose pulses were added according to a mode of cultivation called Segregostat. At this stage, two questions arise i.e., i. Does the Segregostat leads to a reduction of the global phenotypic heterogeneity of the population? and ii. Is it necessary to rely on automated FC for triggering glucose pulses, or can periodic pulsing be considered for this purpose?

To reply to the first question, we previously used information theory for deriving a proxy that can be used for quantifying the degree of heterogeneity of a cell population i.e., the information entropy.[43] The computation of the entropy profile H(t) can be done based on the same binning strategy as the one developed for computing F(t) (Figure S8). The second question was challenged by comparing the Segregostat data to the one obtained in the chemostat and continuous culture where glucose pulses were periodically applied (Figures 5A–5C). Whereas the quantitative measurement of the total amount of biofilm inside the continuous bioreactor is challenging to determine, we can clearly see that, upon Segregostat cultivation, the global entropy profile H(t) is reduced by comparison to standard cultivation or when periodic pulsing is applied (Figure 5D). Indeed, the computation of entropy reveals that, in the Segregostat, the microbial population is more homogeneous and contains mainly PI negative cells, indicating that biofilm switching is less marked in this case.

DISCUSSION

Taken altogether, the data displayed in this work suggest that biofilm switching for *Pseudomonas* sp. is a collective decision taken by cells very early during planktonic growth, this decision being influenced by the amount of eDNA released to the extracellular medium. The transition from a planktonic to a biofilm state in bacterial populations is a complex process influenced by various factors and, accordingly, early cell decision-making process related to the switch to biofilm lifestyle has not been thoroughly investigated so far. However, this study suggests that a subpopulation of cells in planktonic cultures plays a pivotal role in initiating biofilm formation. Indeed, biofilm formation is determined early in the planktonic phase and is correlated with the number of eDNA-associated cells. The same finding has been previously reported for *P. aeruginosa*,[17] suggesting that our methodology could be potentially applied to several other microbial species. Since these cells are associated with eDNA, a simple PI staining can be used for its detection. PI is commonly used in microscopy imaging to visualize eDNA within biofilms or cell aggregates.[4,44,45] It has also been shown that the use of PI as a bacterial viability stain can yield misleading signals of cell death by binding to eDNA,[46] a characteristic that can be exploited for detecting eDNA in biofilms.[4] We observed that the fraction of PI-positive/eDNA-associated cells is correlated with the overall biofilm formation capability of the population. This finding challenges the traditional view of phenotypic switching, where individual cells decide to activate or repress gene circuits based on environmental cues.[31,33] Instead, for *Pseudomonas* sp., biofilm switching appears to be determined on a collective basis, driven by the quantity of eDNA molecules released into the supernatant.

Interestingly, a study conducted by Steinberger et al. revealed that *P. putida* KT2440, specifically, produced a significant amount of eDNA.[47] However, another investigation focused on the presence of eDNA in biofilms at the liquid-solid interface. In this study, 7-day-old flow cell biofilms were examined, comparing TOL-free and TOL-carrying strains of KT2440. It was observed that, for the TOL-carrying strain, eDNA constituted a major component of the biofilm. On the other hand, the plasmid-free strains did not form thick biofilms, and eDNA was not detected.[48] However, our study did not pointed out any increase in eDNA concentration in the strains carrying empty plasmid (*P. putida* KT2440pS638 and *P. putida* Δ*lap*A:pS638) (Figure S4).

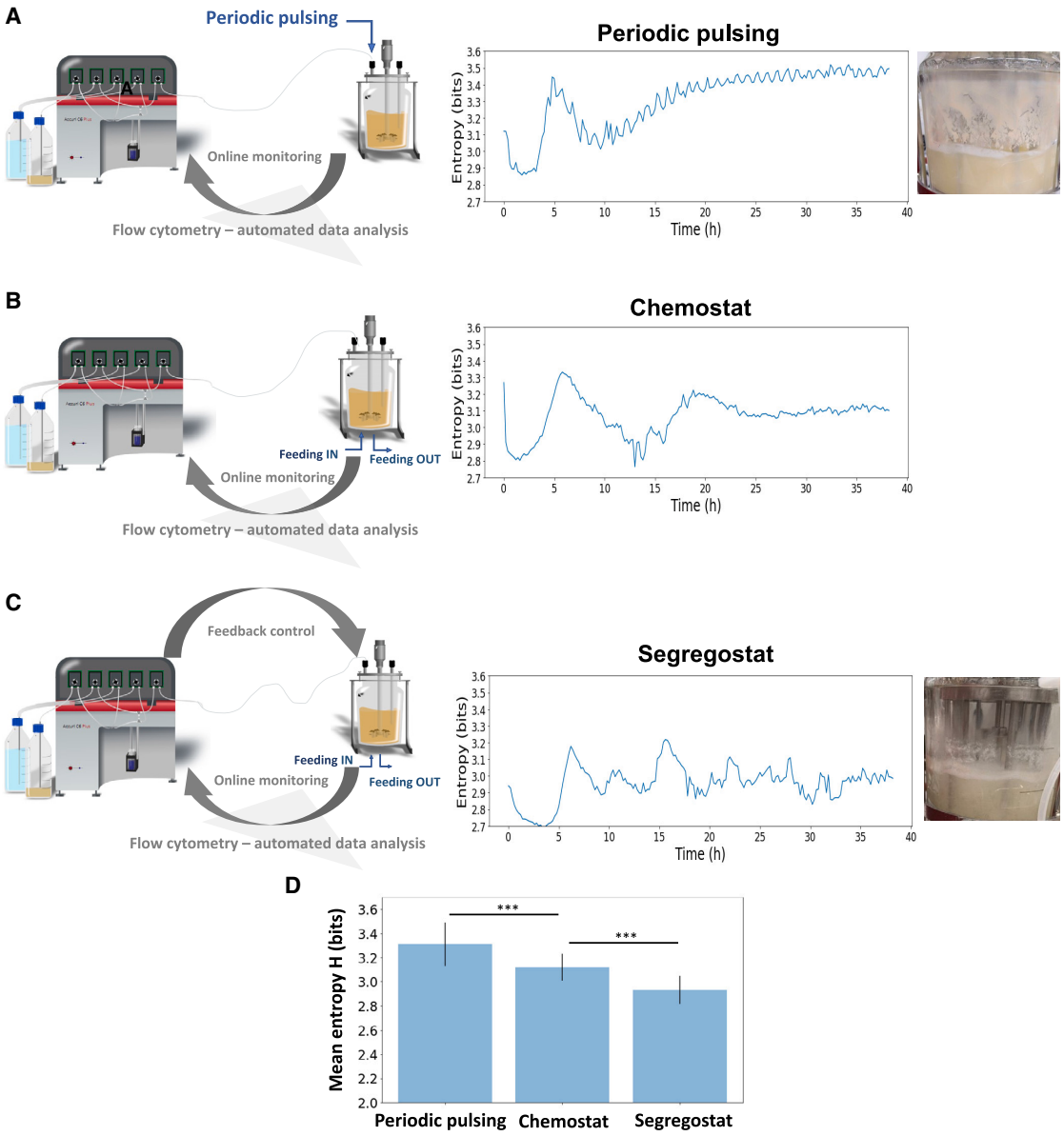

Figure 5. Monitoring and control of biofilm switching based on automated FC

Evolution of the entropy H in (A) Continuous cultivation at a dilution rate of 0.1 h^{-1} with periodic pulsing of glucose (0.5 g L^{-1} of glucose added each hour).

(B) Chemostat cultivation at a dilution rate of 0.1 h^{-1}.

(C) Segregostat cultivation. Pictures of the biofilm formed on the well of the cultivation vessel are shown for the cultivations performed under periodic pulsing and Segregostat cultivations.

(D) Comparative analysis of the mean level of information entropy H for the three modes of cultivation considered (One-way ANOVA test. Data are significantly different with $p < 0.001$, indicated as ***). Results are presented as mean ± standard deviation.

In a separate study by Coronado et al., it was suggested that eDNA may not be a highly relevant component of the biofilm matrix.[49] These contrasting findings indicate that not only do different environmental conditions influence the composition of the extracellular matrix in *P. putida* biofilms, but the presence of the large catabolic plasmid pWW0 may also lead to alterations in the balance of matrix components. These results highlight the need for cross-comparison of data generated using different strains, originally derived from the same but tested and maintained in different conditions laboratories.

Although the mechanism of eDNA release is not yet fully characterized, in Gram-negative bacteria like *Pseudomonas aeruginosa*, the release of eDNA is mediated through various mechanisms. Quorum sensing, involving N-acyl-L-homoserine lactones (AHL) and the *Pseudomonas* quinolone signal (PQS), triggers eDNA release in planktonic cultures by inducing phage

production.[16] Interestingly, recent findings have revealed that eDNA release in *P. aeruginosa* also occurs through oxidative stress caused by the generation of hydrogen peroxide (H2O2) mediated by pyocyanin production.[50] Pyocyanin, a phenazine molecule that is regulated by quorum sensing,[51] facilitates the binding of eDNA to *P. aeruginosa* cells. This association between pyocyanin and eDNA can impact the cell surface properties of *P. aeruginosa*, such as size, hydrophobicity, and surface energies, ultimately influencing cell-to-cell interactions and aggregation. Accordingly, a greater release of eDNA increases the probability of cell binding, which, in turn, promotes cell aggregation and biofilm formation.[52] Recent reports suggest that the presence of eDNA on bacterial cell surfaces promotes surface hydrophobicity and influences attractive acid-base interactions and therewith promotes initial bacterial adhesion and aggregation.[53–55] The dynamics of the process, as cells within the population switch from planktonic to biofilm state, has been characterized based on automated FC. FC offers a rapid and accurate method for quantifying specific cellular subpopulations within a biofilm.[56] Additionally, it has gained popularity to investigate bacterial auto-aggregation.[57,58] PI-positive cells can indeed be easily determined based on FC and can also be used as an early-warning indicator for biofilm formation.

Accordingly, we conducted a more precise characterization of biofilm switching based on automated FC.[39] Automated FC is indeed a valuable tool for monitoring the dynamics of cell population and is used here for tracking changes in the population as it transitions from planktonic to biofilm states.[36] The device can automate environmental transitions based on the phenotypic switching capability of the population.[34,39] In this work, we took benefit from Segregostat and the unique characteristics of eDNA to interfere with the biofilm switching mechanisms according to the detection of the burst of PI-positive cells. Furthermore, we demonstrated that using the environmental forcing implemented by Segregostat cultivation led to detection of the bursts of diversification and leads to a reduction in biofilm formation. Based on this experimental set-up, glucose pulses were administered in response to the detection of diversification bursts associated with PI-positive cells, giving a growth advantage to non-differentiated cells in the liquid phase, thereby controlling phenotypic switching. The results showed that the Segregostat approach reduced the overall heterogeneity of the population, indicating a more homogeneous microbial community with predominantly PI-negative cells, suggesting a decrease in biofilm switching.

The findings offer new perspectives on microbial population dynamics and strategies for controlling biofilm formation. The application of Segregostat cultivation and the use of automated FC for monitoring and intervening in the diversification process open possibilities for more targeted approaches to biofilm mitigation, with potential applications in microbiology and biotechnology.[1,59]

Limitations of the study

This study investigates the early events involved in cell aggregate and biofilm formation in *Pseudomonas putida* KT2440 using a continuous cultivation device coupled with automated FC. FC with PI staining detects cells bound to eDNA, while forward and side-scatter channels measure cell size and auto-aggregation. These aggregates are the initial step toward surface-attached biofilm formation. Although our setup does not allow precise quantification of surface-attached biofilm, our feedback control strategy, which uses glucose pulsing to favor PI-negative cells, significantly reduces aggregates and biofilm attachment on the bioreactor wall (visual inspection).

Our main finding, that controlled glucose pulsing reduces biofilm formation, was demonstrated in a monoculture. However, in natural environments, microbial diversity leads to multi-species biofilms, where microbial interactions influence biofilm formation. A promising follow-up study would be to replicate these experiments in co-culture or synthetic communities, exploring the impact of microbial interactions on biofilm formation.

RESOURCE AVAILABILITY

Lead contact

Further information and requests for resources and reagents should be directed to and will be fulfilled by the lead contact, Frank Delvigne (f.delvigne@uliege.be).

Materials availability

Strains used and plasmids generated in this study are available from the lead contact upon request.

This study did not generate new unique reagents.

Data and code availability

- Data: the automated flow cytometry data have been deposited at Zenodo as https://doi.org/10.5281/zenodo.14229909.
- Code: the codes are available through the link provided in the key resources table.
- DOI, raw confocal microscopy, and any additional information mentioned in this article can be obtained from the lead contact upon request. Any further details necessary for the reanalysis of the data presented in this paper are also accessible from the lead contact upon request.

ACKNOWLEDGMENTS

We gratefully acknowledge Alexandre Hugo (GIGA Institute, Liège, Belgium) for his valuable assistance in performing imaging by scanning electron microscopy. Prof. Victor de Lorenzo, CNB-CSIC, Spain, kindly provided plasmids pSEVA227M and pSEVA227Y. We are also grateful to the company John Cockerill and the Service Public de Wallonie (SPW) for financial support through the Talk2Clean project.

AUTHOR CONTRIBUTIONS

F.B. collected and analyzed data. F.D. and F.B. drafted the article. F.M., D.V., and N.W. contributed to strain construction. F.D., P.N., and A.M. served as scientific advisors and reviewed the study design and article critically.

DECLARATION OF INTERESTS

The authors declare no competing interests.

STAR★METHODS

Detailed methods are provided in the online version of this paper and include the following:

- KEY RESOURCES TABLE
- EXPERIMENTAL MODEL AND STUDY PARTICIPANT DETAILS
- METHOD DETAILS
  - Microbial strains and medium composition

SUPPLEMENTAL INFORMATION

Supplemental information can be found online at https://doi.org/10.1016/j.isci.2025.112063.

Received: December 21, 2023
Revised: June 28, 2024
Accepted: February 14, 2025
Published: February 18, 2025

REFERENCES

1. Philipp, L.-A., Bühler, K., Ulber, R., and Gescher, J. (2024). Beneficial applications of biofilms. Nat. Rev. Microbiol. *22*, 276–290. https://doi.org/10.1038/s41579-023-00985-0.
2. Penesyan, A., Paulsen, I.T., Kjelleberg, S., and Gillings, M.R. (2021). Three faces of biofilms: a microbial lifestyle, a nascent multicellular organism, and an incubator for divers. NPJ Biofilms Microbiomes *7*, 80. https://doi.org/10.1038/s41522-021-00251-2.
3. Sauer, K., Stoodley, P., Goeres, D.M., Hall-Stoodley, L., Burmølle, M., Stewart, P.S., and Bjarnsholt, T. (2022). The biofilm life cycle: expanding the conceptual model of biofilm formation. Nat. Rev. Microbiol. *20*, 608–620. https://doi.org/10.1038/s41579-022-00767-0.
4. Secchi, E., Savorana, G., Vitale, A., Eberl, L., Stocker, R., and Rusconi, R. (2022). The structural role of bacterial eDNA in the formation of biofilm streamers. Proc. Natl. Acad. Sci. USA *119*, e2113723119.
5. Cai, Y.-M. (2020). Non-surface Attached Bacterial Aggregates: A Ubiquitous Third Lifestyle. Front. Microbiol. *11*, 557035. https://doi.org/10.3389/fmicb.2020.557035.
6. Kragh, K.N., Tolker-Nielsen, T., and Lichtenberg, M. (2023). The non-attached biofilm aggregate. Commun. Biol. *6*, 898. https://doi.org/10.1038/s42003-023-05281-4.
7. Kragh, K.N. (2018). The Inoculation Method Could Impact the Outcome of Microbiological Experiments. Appl. Environ. Microbiol. *84*, e02264.
8. Schleheck, D. (2009). Pseudomonas aeruginosa PAO1 Preferentially Grows as Aggregates in Liquid Batch Cultures and Disperses upon Starvation. PLoS One *4*, e5513.
9. Laganenka, L. (2016). Chemotaxis towards autoinducer 2 mediates autoaggregation in Escherichia coli. Nature Communication *7*, 12984.
10. Perez-Soto, N., Creese, O., Fernandez-Trillo, F., and Krachler, A.M. (2018). Aggregation of Vibrio cholerae by Cationic Polymers Enhances Quorum Sensing but Overrides Biofilm Dissipation in Response to Autoinduction. ACS Chem. Biol. *13*, 3021–3029.
11. Chandler, J.R., Duerkop, B.A., Hinz, A., West, T.E., Herman, J.P., Churchill, M.E.A., Skerrett, S.J., and Greenberg, E.P. (2009). Mutational Analysis of Burkholderia thailandensis Quorum Sensing and Self-Aggregation. J. Bacteriol. *191*, 5901–5909.
12. Das, T., Sehar, S., Koop, L., Wong, Y.K., Ahmed, S., Siddiqui, K.S., and Manefield, M. (2014). Influence of Calcium in Extracellular DNA Mediated Bacterial Aggregation and Biofilm Formation. PLoS One *9*, e91935. https://doi.org/10.1371/journal.pone.0091935.
13. Qin, Z., Ou, Y., Yang, L., Zhu, Y., Tolker-Nielsen, T., Molin, S., and Qu, D. (2007). Role of autolysin-mediated DNA release in biofilm formation of Staphylococcus epidermidis. Microbiology (N. Y.) *153*, 2083–2092.
14. Whitchurch, C.B., Tolker-Nielsen, T., Ragas, P.C., and Mattick, J.S. (2002). Extracellular DNA Required for Bacterial Biofilm Formation. Science *295*, 1487.
15. Moscoso, M., García, E., and López, R. (2006). Biofilm Formation by Streptococcus pneumoniae: Role of Choline, Extracellular DNA, and Capsular Polysaccharide in Microbial Accretion. J. Bacteriol. *188*, 7785–7795. https://doi.org/10.1128/JB.00673-06.
16. Allesen-Holm, M., Barken, K.B., Yang, L., Klausen, M., Webb, J.S., Kjelleberg, S., Molin, S., Givskov, M., and Tolker-Nielsen, T. (2006). A characterization of DNA release in Pseudomonas aeruginosa cultures and biofilms. Mol. Microbiol. *59*, 1114–1128.
17. Hynen, A.L., Lazenby, J.J., Savva, G.M., McCaughey, L.C., Turnbull, L., Nolan, L.M., and Whitchurch, C.B. (2021). Multiple holins contribute to extracellular DNA release in Pseudomonas aeruginosa biofilms. Microbiology *167*, 000990.
18. Nagler, M., Insam, H., Pietramellara, G., and Ascher-Jenull, J. (2018). Extracellular DNA in natural environments: features, relevance and applications. Appl. Microbiol. Biotechnol. *102*, 6343–6356.
19. Gloag, E.S., Turnbull, L., Huang, A., Vallotton, P., Wang, H., Nolan, L.M., Mililli, L., Hunt, C., Lu, J., Osvath, S.R., et al. (2013). Self-organization of bacterial biofilms is facilitated by extracellular DNA. Proc. Natl. Acad. Sci. USA *110*, 11541–11546.
20. Pakkulnan, R., Anutrakunchai, C., Kanthawong, S., Taweechaisupapong, S., Chareonsudjai, P., and Chareonsudjai, S. (2019). Extracellular DNA facilitates bacterial adhesion during Burkholderia pseudomallei biofilm formation. PLoS One *14*, e0213288. https://doi.org/10.1371/journal.pone.0213288.
21. Mlynek, K.D., Bulock, L.L., Stone, C.J., Curran, L.J., Sadykov, M.R., Bayles, K.W., and Brinsmade, S.R. (2020). Genetic and Biochemical Analysis of CodY-Mediated Cell Aggregation in Staphylococcus aureus Reveals an Interaction between Extracellular DNA and Polysaccharide in the Extracellular Matrix. J. Bacteriol. *202*, 10–1128. https://doi.org/10.1128/JB.00593-19.
22. Benedetti, I., de Lorenzo, V., and Nikel, P.I. (2016). Genetic programming of catalytic Pseudomonas putida biofilms for boosting biodegradation of haloalkanes. Metab. Eng. *33*, 109–118. https://doi.org/10.1016/j.ymben.2015.11.004.
23. Nikel, P.I., Martínez-García, E., and de Lorenzo, V. (2014). Biotechnological domestication of Pseudomonads using synthetic biology. Nat. Rev. Microbiol. *12*, 368–379. https://doi.org/10.1038/nrmicro3253.
24. Volke, D.C., Friis, L., Wirth, N.T., Turlin, J., and Nikel, P.I. (2020). Synthetic control of plasmid replication enables target- and self-curing of vectors and expedites genome engineering of Pseudomonas putida. Metab. Eng. Commun. *10*, e00126. https://doi.org/10.1016/j.mec.2020.e00126.
25. Weimer, A., Kohlstedt, M., Volke, D.C., Nikel, P.I., and Wittmann, C. (2020). Industrial biotechnology of Pseudomonas putida: advances and prospects. Appl. Microbiol. Biotechnol. *104*, 7745–7766. https://doi.org/10.1007/s00253-020-10811-9.
26. Espinosa-Urgel, M., and Ramos-González, M.I. (2023). Becoming settlers: Elements and mechanisms for surface colonization by Pseudomonas putida. Environ. Microbiol. *25*, 1575–1593. https://doi.org/10.1111/1462-2920.16385.
27. Fernández, A.J. (2014). Regulation of the lifestyle switch in Pseudomonas putida. Memoria Presentada Por, 177.
28. Gjermansen, M., Nilsson, M., Yang, L., and Tolker-Nielsen, T. (2010). Characterization of starvation-induced dispersion in Pseudomonas putida

biofilms: genetic elements and molecular mechanisms mmi_6793 815.826. Mol. Microbiol. *75*, 815–826. https://doi.org/10.1111/j.1365-2958.2009.06793.x.

29. Martı'nez-Gil, M. (2013). Interplay between extracellular matrix components of Pseudomonas putida biofilms. Res. Microbiol. *164*, 382–389. https://doi.org/10.1016/j.resmic.2013.03.021.
30. Nilsson, M. (2011). nfluence of putative exopolysaccharide genes on Pseudomonas putida KT2440 biofilm stability. Environ. Microbiol. *5*, 1357–136913. https://doi.org/10.1111/j.1462-2920.2011.02447.x.
31. Kussell, E., and Leibler, S. (2005). Phenotypic Diversity, Population Growth, and Information in Fluctuating Environments. Science *309*, 2075–2078.
32. Acar, M., Mettetal, J.T., and van Oudenaarden, A. (2008). Stochastic switching as a survival strategy in fluctuating environments. Nat. Genet. *40*, 471–475. https://doi.org/10.1038/ng.110.
33. Thattai, M., and van Oudenaarden, A. (2004). Stochastic Gene Expression in Fluctuating Environments. Genetics Society of America *167*, 523–530.
34. Henrion, L., Martinez, J.A., Vandenbroucke, V., Delvenne, M., Telek, S., Zicler, A., Grünberger, A., and Delvigne, F. (2023). Fitness cost associated with cell phenotypic switching drives population diversification dynamics and controllability. Nat. Commun. *14*, 6128. https://doi.org/10.1038/s41467-023-41917-z.
35. Bertaux, F., Sosa-Carrillo, S., Gross, V., Fraisse, A., Aditya, C., Furstenheim, M., and Batt, G. (2022). Enhancing bioreactor arrays for automated measurements and reactive control with ReacSight. Nat. Commun. *13*, 3363. https://doi.org/10.1038/s41467-022-31033-9.
36. Martinez, F.D.a.J.A. (2023). Advances in automated and reactive flow cytometry for synthetic biotechnology. Curr. Opin. Biotechnol. *83*, 102974. https://doi.org/10.1016/j.copbio.2023.102974.
37. Shi, L., Günther, S., Hübschmann, T., Wick, L.Y., Harms, H., and Müller, S. (2007). Limits of Propidium Iodide as a Cell Viability Indicator for Environmental Bacteria. Cytometry. A. *71*, 592–598. https://doi.org/10.1002/cyto.a.20402.
38. Davey, H.M., and Hexley, P. (2011). Red but not dead? Membranes of stressed Saccharomyces cerevisiae are permeable to propidium iodide. Environ. Microbiol. *13*, 163–171. https://doi.org/10.1111/j.1462-2920.2010.02317.x.
39. Sassi, H., Nguyen, T.M., Telek, S., Gosset, G., Grünberger, A., and Delvigne, F. (2019). Segregostat: a novel concept to control phenotypic diversification dynamics on the example of Gram-negative bacteria. Microb. Biotechnol. *12*, 1064–1075. https://doi.org/10.1111/1751-7915.13442.
40. Baert, J., Delepierre, A., Telek, S., Fickers, P., Toye, D., Delamotte, A., Lara, A.R., Jaén, K.E., Gosset, G., Jensen, P.R., and Delvigne, F. (2016). Microbial population heterogeneity versus bioreactor heterogeneity: evaluation of Redox Sensor Green as an exogenous metabolic biosensor. Eng. Life Sci. *16*, 643–651. https://doi.org/10.1002/elsc.201500149.
41. Okshevsky, M., and Meyer, R.L. (2014). Evaluation of fluorescent stains for visualizing extracellular DNA in biofilms. J. Microbiol. Methods *105*, 102–104. https://doi.org/10.1016/j.mimet.2014.07.010.
42. Gjermansen, M., Ragas, P., and Tolker-Nielsen, T. (2006). Proteins with GGDEFand EAL domains regulate Pseudomonas putida biofilm formationand dispersal. FEMS Microbiol. Lett. *265*, 215–224. https://doi.org/10.1111/j.1574-6968.2006.00493.x.
43. Henrion, L., Delvenne, M., Bajoul Kakahi, F., Moreno-Avitia, F., and Delvigne, F. (2022). Exploiting Information and Control Theory for Directing Gene Expression in Cell Populations. Front. Microbiol. *13*, 869509.
44. Deng, S. (2020). Novel Bacterial Diversity and Fragmented eDNA Identified in Hyperbiofilm-Forming Pseudomonas aeruginosa Rugose Small Colony Variant. iScience *23*, 100827. https://doi.org/10.1016/j.isci.2020.100827.
45. Moshynets, O.V., Pokholenko, I., Iungin, O., Potters, G., and Spiers, A.J. (2022). eDNA, Amyloid Fibers and Membrane Vesicles Identified in Pseudomonas fluorescens SBW25 Biofilms. Int. J. Mol. Sci. *23*, 15096. https://doi.org/10.3390/ijms232315096.
46. Rosenberg, M., Azevedo, N.F., and Ivask, A. (2019). Propidium iodide staining underestimates viability of adherent bacterial cells. Sci. Rep. *9*, 6483. https://doi.org/10.1038/s41598-019-42906-3.
47. Steinberger, R.E., and Holden, P.A. (2005). Extracellular DNA in Single- and Multiple-Species Unsaturated Biofilms. Appl. Environ. Microbiol. *71*, 5404–5410. https://doi.org/10.1128/AEM.71.9.5404–5410.2005.
48. D'Alvise, P.W., Sjøholm, O.R., Yankelevich, T., Jin, Y., Wuertz, S., and Smets, B.F. (2010). TOLplasmid carriage enhances bio¢lm formationand increases extracellularDNAcontent inPseudomonasputidaKT2440. FEMS Microbiol. Lett. *312*, 84–92. https://doi.org/10.1111/j.1574-6968.2010.02105.x.
49. Yousef-Coronado, F., Travieso, M.L., and Espinosa-Urgel, M. (2008). Different, overlappingmechanisms for colonizationofabiotic and plant surfacesbyPseudomonasputida. FEMS Microbiol. Lett. *288*, 118–124. https://doi.org/10.1111/j.1574-6968.2008.01339.x.
50. Das, T., and Manefield, M. (2012). Pyocyanin Promotes Extracellular DNA Release in Pseudomonas aeruginosa. PLoS One *7*, e46718. https://doi.org/10.1371/journal.pone.0046718.
51. Price-Whelan, A., Dietrich, L.E.P., and Newman, D.K. (2006). Rethinking 'secondary' metabolism: physiological roles for phenazine antibiotics. Nat. Chem. Biol. *2*, 71–78. https://doi.org/10.1038/nchembio764.
52. Secor, P.R., Michaels, L.A., Ratjen, A., Jennings, L.K., and Singh, P.K. (2018). Entropically driven aggregation of bacteria by host polymers promotes antibiotic tolerance in Pseudomonas aeruginosa. Proc. Natl. Acad. Sci. USA *115*, 10780–10785.
53. Das, T., Sharma, P.K., Busscher, H.J., van der Mei, H.C., and Krom, B.P. (2010). Role of Extracellular DNA in Initial Bacterial Adhesion and Surface Aggregation. Appl. Environ. Microbiol. *76*, 3405–3408. https://doi.org/10.1128/AEM.03119-09.
54. Das, T., Krom, B.P., van der Mei, H.C., Busscher, H.J., and Sharma, P.K. (2011). DNA-mediated bacterial aggregation is dictated by acid–base interactions. Soft Matter *7*, 2927. https://doi.org/10.1039/c0sm01142h.
55. Liu, H.-H., Yang, Y.R., Shen, X.C., Zhang, Z.L., Shen, P., and Xie, Z.X. (2008). Role of DNA in Bacterial Aggregation. Curr. Microbiol. *57*, 139–144. https://doi.org/10.1007/s00284-008-9166-0.
56. Kerstens, M., Boulet, G., Van Kerckhoven, M., Clais, S., Lanckacker, E., Delputte, P., Maes, L., and Cos, P. (2015). A flow cytometric approach to quantify biofilms. Folia Microbiol. *60*, 335–342. https://doi.org/10.1007/s12223-015-0400-4.
57. Tomich, M., and Mohr, C.D. (2003). Adherence and autoaggregation phenotypes of a Burkholderia cenocepacia cable pilus mutant. FEMS Microbiol. Lett. *228*, 287–297. https://doi.org/10.1016/S0378-1097(03)00785-7.
58. Espeso, D.R., Martínez-García, E., and de Lorenzo, V. (2021). Quantitative assessment of morphological traits of planktonic bacterial aggregates. Water Res. *188*, 116468. https://doi.org/10.1016/j.watres.2020.116468.
59. Halan, B., Buehler, K., and Schmid, A. (2012). Biofilms as living catalysts in continuous chemical syntheses. Trends Biotechnol. *30*, 453–465. https://doi.org/10.1016/j.tibtech.2012.05.003.
60. Wirth, N.T., Kozaeva, E., and Nikel, P.I. (2020). Accelerated genome engineering of Pseudomonas putida by I-SceI—mediated recombination and CRISPR-Cas9 counterselection. Microb. Biotechnol. *13*, 233–249. https://doi.org/10.1111/1751-7915.13396.
61. Cavaleiro, A.M., Kim, S.H., Seppälä, S., Nielsen, M.T., and Nørholm, M.H.H. (2015). Accurate DNA Assembly and Genome Engineering with Optimized Uracil Excision Cloning. ACS Synth. Biol. *4*, 1042–1046. https://doi.org/10.1021/acssynbio.5b00113.
62. Choi, K.-H., Kumar, A., and Schweizer, H.P. (2006). A 10-min method for preparation of highly electrocompetent Pseudomonas aeruginosa cells: Application for DNA fragment transfer between chromosomes and plasmid transformation. J. Microbiol. Methods *64*, 391–397. https://doi.org/10.1016/j.mimet.2005.06.001.
63. Ren, D., Madsen, J.S., de la Cruz-Perera, C.I., Bergmark, L., Sørensen, S.J., and Burmølle, M. (2014). High-Throughput Screening ofMultispecies

Biofilm Formation and Quantitative PCR-Based Assessment of Individual Species Proportions, Useful for Exploring Interspecific Bacterial Interactions. Microb. Ecol. *68*, 146–154. https://doi.org/10.1007/s00248-013-0315-z.

64. Velastegui, E., Quezada, J., Guerrero, K., Altamirano, C., Martinez, J.A., Berrios, J., and Fickers, P. (2023). Is heterogeneity in large-scale bioreactors a real problem in recombinant protein synthesis by Pichia pastoris? Appl. Microbiol. Biotechnol. *107*, 2223–2233. https://doi.org/10.1007/s00253-023-12434-2.

65. Nguyen, T.M., Telek, S., Zicler, A., Martinez, J.A., Zacchetti, B., Kopp, J., Slouka, C., Herwig, C., Grünberger, A., and Delvigne, F. (2021). Reducing phenotypic instabilities of a microbial population during continuous cultivation based on cell switching dynamics. Biotechnol. Bioeng. *118*, 3847–3859. https://doi.org/10.1002/bit.27860.

66. Christen, M., Kulasekara, H.D., Christen, B., Kulasekara, B.R., Hoffman, L.R., and Miller, S.I. (2010). Asymmetrical Distribution of the Second Messenger c-di-GMP upon Bacterial Cell Division. Science *328*, 1295–1297. https://doi.org/10.1126/science.1188658.

67. Dusny, C., and Schmid, A. (2015). Microfluidic single-cell analysis links boundary environments and individual microbial phenotypes. Environ. Microbiol. *17*, 1839–1856.

68. Binder, D., Drepper, T., Jaeger, K.E., Delvigne, F., Wiechert, W., Kohlheyer, D., and Grünberger, A. (2017). Homogenizing bacterial cell factories: Analysis and engineering of phenotypic heterogeneity. Metab. Eng. *42*, 145–156. https://doi.org/10.1016/j.ymben.2017.06.009.

69. Ladner, T., Grünberger, A., Probst, C., Kohlheyer, D., Büchs, J., and Delvigne, F. (2017). Application of Mini- and Micro-Bioreactors for Microbial Bioprocesses. In Current Developments in Biotechnology and Bioengineering: Bioprocesses, Bioreactors and Controls (Elsevier), pp. 433–461. https://doi.org/10.1016/B978-0-444-63663-8.00015-X.

70. Zid, B.M., and O'Shea, E.K. (2014). Promoter sequences direct cytoplasmic localization and translation of mRNAs during starvation in yeast. Nature *514*, 117–121. https://doi.org/10.1038/nature13578.

71. Tostevin, F., and ten Wolde, P.R. (2009). Mutual information between input and output trajectories of biochemical networks. Phys. Rev. Lett. *102*, 218101. https://doi.org/10.1103/PhysRevLett.102.218101.

72. Cheong, R., Rhee, A., Wang, C.J., Nemenman, I., and Levchenko, A. (2011). Information transduction capacity of noisy biochemical signaling networks. Science *334*, 354–358.

73. Tan, C., Reza, F., and You, L. (2007). Noise-limited frequency signal transmission in gene circuits. Biophys. J. *93*, 3753–3761. https://doi.org/10.1529/biophysj.107.110403.

74. Perkins, T.J., and Swain, P.S. (2009). Strategies for cellular decision-making. Mol. Syst. Biol. *5*, 326. https://doi.org/10.1038/msb.2009.83.

75. Bowsher, C.G., and Swain, P.S. (2014). Environmental sensing, information transfer, and cellular decision-making. Curr. Opin. Biotechnol. *28*, 149–155. https://doi.org/10.1016/j.copbio.2014.04.010.

STAR★METHODS

KEY RESOURCES TABLE

REAGENT or RESOURCE	SOURCE	IDENTIFIER
Bacterial		
E. coli DH5α λpir	Platt et al.[60]	Cloning host; F– λ– endA1 glnX44(AS) thiE1 recA1 relA1 spoT1 gyrA96(Nal^R) rfbC1 deoR nupGΦ80(lacZΔM15) Δ(argF-lac)U169 hsdR17(rK– mK+), λpir lysogen
P. putida KT2440	Bagdasarian et al.[61]	Wild-type strain, derived from *P. putida* mt-2 (Worsey and Williams et al[62])cured of the TOL plasmid pWW0
P. putida Δ*lap*A	This paper	Derivate of *P. putida* KT2440 with a clean deletion of *lap*A (PP_0168)
P. putida DGC	This paper	Derivate of *P. putida* KT2440 harboring the plasmid pS638::DGC-244
Recombinant DNA		
pGNW2·Δ*lap*A	This paper	Derived from pGNW2 with homologous flanking region to *lap*A (PP_0168)
pSEVA638	Martínez-Garćía et al.[63]	oriV(pBBR1); XylS/Pm→multiple cloning site (MCS); GmR
pS638::DGC-244	This paper	Derived from pSEVA638 with insertion of DGC-244 into the MCS
pGNW2	Wirth et al.[64]	oriV(R6K); PEM14gBCD→msfGFP; KmR
pSEVA227M	Silva-Rocha et al.[65]	KmR; ori (RK2), Pem7 – msf.GFP
pSEVA227Y	Silva-Rocha et al.[65]	KmR; ori (RK2), pBG 17– YFP
P. putida Δ*lap*A::pS638	This paper	Strain with empty plasmid
P. putida KT2440::pS638	This paper	Strain with empty plasmid
Oligonucleotides		
Amplification of *dgc*A0240, Amplification of genomic regions adjacent to lapA, see Table S1	This paper	Provided by Prof. Pablo Iván Nikel (DTU)
Chemicals, peptides, and recombinant proteins		
Propidium iodide	Sigma-Aldrich	B34954B
Redox Sensor Green	Sigma-Aldrich	B34954
Crystal violet	Merck	C.I. 42555
TOTO^{TM}-1 iodide	Invitrogen^{TM} Thermo Fisher Scientific	T3600
SYTO^{TM}9	Invitrogen^{TM} Thermo Fisher Scientific	S34854
SYTO^{TM}60	Invitrogen^{TM} Thermo Fisher Scientific	S11342
QuantiFluor dsDNA System	Promega, Madison, WI, USA	E2670
Gentamicin	Sigma-Aldrich	G1914-5G
Kanamycin	InvitrogenTM Thermo Fisher Scientific	11815024
Protein precipitation solution	Promega, USA	A795A
Lambda DNA	InvitrogenTM Molecular Probes	HY-KE7067
BamHI	Thermo Fisher Scientific	FD0054
SacI	Thermo Fisher Scientific	FD1133
NucleoSpin Gel and PCR Clean-up Columns	Macherey Nage	
T4 DNA ligase	Thermo Fisher Scientific	EL0014
OneTaq® 2X Master Mix	New England Biolabs	N/A
NucleoSpin Plasmid	EasyPure, Germany	N/A
Attune performance tracking beads	Thermo Fisher, USA	C36950/LOT # 2054455

(*Continued on next page*)

Continued

REAGENT or RESOURCE	SOURCE	IDENTIFIER
DNase I	Roche	04716728001
Biotin	Sigma-Aldrich	SLCP 6816
Thiamin	Sigma-Aldrich	LOT # BCCD1177
Deposited data		
Raw data	This paper	https://doi.org/10.5281/zenodo.14229909
Software and algorithms		
GraphPad Prism 8.0.1	Prism	https://www.graphpad.com/
ImageJ	Fiji software	https://imagej.nih.gov/ij/
MATLAB 2023	Mathworks	
MiPI Flow Cytometry Analysis toolbox (mFCAtoolbox)	This paper	https://gitlab.uliege.be/mipi/published-software/2024-bajoul

EXPERIMENTAL MODEL AND STUDY PARTICIPANT DETAILS

Pseudomonas putida KT2440 was used as the main microbial chassis throughout this study. Derivatives of this strain i.e., *P. putida* Δ*lap*A and *P. putida* DGC, were obtained by genetic manipulation (see method details – plasmid design and genetic manipulations). All bacterial strains used in this study are listed in the key resources table.

METHOD DETAILS

Microbial strains and medium composition

All strains were maintained in 25% (v/v) glycerol at –80°C in working seed vials (2 mL). Prior to experiments, one colony of each bacterium was used to inoculate 10 mL of lysogeny broth (LB) medium (10 g L^{-1} NaCl, 5 g L^{-1} yeast extract, and 12 g L^{-1} tryptone) and grown for 6 h with shaking at 30°C. Precultures and cultures of all bacteria were done in modified M9 minimal medium (33.7 mM Na_2HPO_4, 22.0 mM KH_2PO_4, 8.55 mM 6 NaCl, 9.35 mM NH_4Cl, 1 mM $MgSO_4$, and 0.3 mM $CaCl_2$), complemented with a trace element (13.4 mM EDTA, 3.1 mM $FeCl_3 \cdot 6H2O$, 0.62 mM $ZnCl_2$, 76 μM $CuCl_2 \cdot 2H_2O$, 42 μM $CoCl_2 \cdot 2H_2O$, 162 μM H_3BO_3, and 8.1 μM $MnCl_2 \cdot 4H2O$), 1 μg L^{-1} biotin and 1 μg L^{-1} thiamin) and supplemented with glucose (5 g L^{-1}) as the main carbon source (pH = 7.2). For strain DGC, the media was supplemented with gentamycin at a final concentration of 10 μg ml^{-1}.

Plasmid design and genetic manipulations

Plasmid pS638::DGC was constructed by amplifying the hyperactive diguanylate cyclase mutant A0244 from Caulobacter crescentus,[66] with the primer pair P1 and P2. The resulting amplicon and vector pSEVA638 were digested with BamHI and SacI (FD0054 and FD1133, Thermo Fisher Scientific). The fragments were purified (NucleoSpin Gel and PCR Clean-up Columns, Macherey Nagel) and ligated with T4 DNA ligase (EL0014, Thermo Fisher Scientific). *E. coli* DH5α was transformed with the ligation mixture and the cell suspension was plated on a gentamycin–selective plate. Subsequently, the constructed pS638::DGC (where DGCA0244 was placed under transcriptional control of the inducible XylS/Pm expression system) plasmid was isolated from a single colony and its correctness was confirmed by sequencing. The plasmids for the deletion of *lap*A were constructed according to a previous study.[60] In short, ∼500 bp homology arms (HA) flanking the gene coding sequences were amplified from the chromosomal DNA of *P. putida* KT2440 using the primer pair P5/P6 (lapA_HA1) and assembled into the suicide vector pSNW2 employing the USER cloning method.[61] The purified plasmids were introduced into stationary *P. putida* KT2440 cells by electroporation and selected on LB agar medium supplemented with kanamycin (50 μg mL-1). The corresponding pSNW2 derivative, now fully integrated into the bacterial chromosome, was resolved by transforming the cells with the auxiliary plasmid pQURE6 and selection on gentamicin (10 μg mL-1) and 3-methyl benzoate (1 mM).[24] Resolved strains (GFP-negative and kanamycin-sensitive) were tested for the desired genotype by colony PCR (OneTaq® 2X Master Mix with Standard Buffer, New England Biolabs). All the plasmids are listed in key resources table.

Plasmid transformation

Plasmids pSEVA227M and pSEVA227Y, propagated in *E. coli* and *P. putida* KT2440 (kindly provided by Prof. Victor de L orenzo, CNB-CSIC, Spain), were isolated with a plasmid extraction kit (NucleoSpin Plasmid EasyPure, Germany) according to the manufacturer's protocol and stored at -20°C. Electrocompetent cells of *P. putida* Δ*lap*A were prepared according to a slightly modified procedure originally described by.[62] Briefly, 1 ml of cells in the early stationary phase (OD_{600} = 1–1.5) from cultures grown in LB medium were harvested by centrifugation at 8000×g and washed twice with 1 ml of 300 mM sucrose at room temperature (RT). Cells were resuspended in 100 μl of 300 mM sucrose. In the case of *P. putida* DGC, electrocompetent cells were prepared by washing the

biomass with 10% (v/v) glycerol. Briefly, 50 ml of a cell culture in the exponential phase (OD600 = 0.8) in LB medium were harvested by centrifugation at 8000×g and washed twice with 50 ice-cold glycerol, centrifuge and resuspend cells in 0.8 ml ice-cold glycerol, keep on ice. Then 50 μl of electrocompetent cells were mixed with 1 μl plasmid DNA (50 ng/ μl) in a 1 mm electroporation cuvette. High voltage electroporation was performed using a Gene Pulser Xcell (Bio-Rad Gene Pulser, US) at 25 μF, 200 Ω, and 1600 kV. After applying the pulse, 1 ml of SOC medium was added immediately, and the cells were transferred to a culture tube and incubated at 30°C for 1 h. Cells were plated on LB agar plates supplemented with 50 μg/mL of kanamycin and incubated at 30°C for 48–72 h.

DNase enzyme treatment

Biofilm and planktonic cell densities were adjusted to (1×10^7 cells mL^{-1}), and samples were resuspended in 500 μL of 1× DNase I buffer (10 mM Tris·HCl, pH = 7.5, 2.5 mM MgCl2, and 0.1 mM CaCl2) with or without DNase I (final concentration 160 U mL^{-1}, Roche, reference number 04716728001) and were incubated at 37°C 10 for 3 h. After incubation, samples were pelleted by centrifugation at 8500 rpm for 10 min, resuspended in PBS, stained by PI, and analyzed by FCM.

Bacterial cultivation

Before initiating the experiments, the *P. putida DGC* strain was grown on LB agar overnight at 30°C. Subsequently, A single colony of bacteria was then used to inoculate 10mL of lysogeny broth (LB) medium, which consisted of 10 g L^{-1} NaCl, 5 g L^{-1} yeast extract, and 4 and 12 g L^{-1} tryptone, and grown overnight hours at 30°C with shaking at 170rpm. Both the precultures and cultures were performed on a defined mineral salt medium (MM9), as detailed earlier. The medium was supplemented with 5 g L^{-1} of glucose as the main carbon source, and the pH was adjusted to 7.2. Additionally, gentamycin was added at a final concentration of 10 μg ml^{-1}. The experimental setup involved three biological replicates, with samples collected from each flask at 6 hours of cultivation for subsequent microscopy analysis.

To assess the viability of subpopulations during 24h cultivation, we performed Redox Sensor Green (RSG) staining. *P. putida* KT2440 and *P. putida* DGC were cultivated for 24h, and samples were collected at time intervals of 6h (early exponential phase), 10h (late exponential phase), and 24h (stationary phase). They were stained with propidium iodide (PI) and Redox Sensor Green (RSG) and subjected to FC analysis.

Staining protocols

In this study, four fluorescent stains were employed: (i) Propidium iodide (PI) (P4170, Sigma-Aldrich); a stock solution was prepared at 1 mg mL^{-1} in sterile Milli-Q water and used at a final concentration of 1.5 μM in sterilized PBS; (ii) TOTO™-1 iodide (T3600, Invitrogen™ Thermo Fisher Scientific); a stock solution was prepared in DMSO (at 1 mM) and used at a final concentration of 2 μM in sterilized PBS; (iii) SYTO™9 (S34854, Invitrogen™ Thermo Fisher Scientific); a stock solution was prepared in DMSO at 5 mM and used at a final concentration of 5 μM in sterilized PBS; and (iv) SYTO™60 (S11342, Invitrogen™ Thermo Fisher Scientific); a stock solution was prepared in DMSO at 5 mM and used at a final concentration of 10 μM in sterilized PBS. For Redox Sensor Green (RSG), a stock solution was prepared at 1 mg mL^{-1} in sterile Milli-Q water and used at a final concentration of 1.5 μM in sterilized PBS.

All bacterial samples were stained right before microscopy imaging analysis by adding 1 μL of the PI stock solution to 1 mL of a cell suspension in PBS ($1X10^7$ cells mL^{-1}). Before CLSM analysis, Staining was performed with one or more fluorescent dyes in the following combinations: PI, SYTO9+PI, and TOTO1+SYTO60. An aliquot of 10-15 μL of 1:1 stain mixture solution has been added to a sample of planktonic and incubated under the exclusion of light (10 min for PI, SYTO9+PI, and 20 min for TOTO1+SYTO60). Controls were also prepared, with live-dead gating based on heat-killed bacteria at 80°C for 1 hour.

Confocal laser scanning microscopy (CLSM)

All samples were analyzed by CLSM with a LSM880 Airyscan super-resolution system (Carl Zeiss, Oberkochen, Germany). The images were taken based on a Plan- Apochromat 63×/1.4 Oil objective. We used an excitation wavelength of 488 nm and emission at 500-550 nm for green fluorescence and an excitation wavelength of 561 nm and emission at 580-18 615 nm for red fluorescence. Images were acquired continuously at a pixel resolution of 0.04 μm (regular Airyscan mode) in XY and 1-μm interval in Z step-size using the piezo drive.

Quantification of biofilm growth in 96-well plates

Two-day biofilm formation of *Pseudomonas* strains was determined by crystal violet staining using a 96-well plate lid with pegs extending into each well (Nunc-TSP lid, Invitrogen™ Thermo Fisher Scientific). Briefly, precultures were grown overnight at 30°C to an OD600 nm of 1.0. The cell suspensions were then adjusted to an OD600 nm of 0.1 in M9 medium. A total of 160 μL cell suspension were added to each well. Fresh medium was used as a negative control. The plates were sealed with parafilm and incubated with shaking at 180 rpm at 30°C. The biofilm biomass was quantified with a crystal violet staining assay modified from previously reported CV assays.[63] CV quantification was performed on the pegs of the Nunc-TSP lid culture system. Briefly, after 48 h of cultivation, the peg lids were taken out and washed three times using PBS. Subsequently, the peg lids were placed in plates with 180 μL of an aqueous 1% (w/v) CV solution. Then, the lids were washed with PBS three times after staining for 20 min. Subsequently, the peg lids with crystal violet stain were placed into a new microtiter plate with 200 μL of 33% (w/v) glacial acetic acid in each well for

15 min. The optical density at 590 nm of each sample was measured by a microplate reader (Tecan SPARK, Männedorf, Switzerland). For each condition, three independent experiments were performed.

Quantification of eDNA production in planktonic cultures

The bacterial strains, including *P. putida* KT2440, *P. putida* ΔlapA, and *P. putida* DGC, were cultured in modified M9 medium in 500mL Erlenmeyer flasks. These flasks were filled up to one-fifth of their nominal volume and placed on a rotary shaker at 170 min^{-1} at 30°C. The shake flasks were grown in parallel under identical conditions for a period of 30 hours, during which biomass growth and eDNA production were monitored. The cell density was estimated by measuring the OD600 nm (Genesys™ 10 UV-Vis, Thermo Scientific, USA). The eDNA in the supernatant was quantified after precipitation. To achieve this, bacterial cells were removed from 900 μL culture through centrifugation (4 min, 6800 g, Eppendorf™ 5424R). The supernatant (700 μL) was transferred to a sterile Eppendorf tube and mixed with 50 μL protein precipitation solution (Promega, USA) by inverting it ten times before centrifugation (10 min, 12100 g, Eppendorf™ 5424R). Then, 700 μL of the supernatant was mixed with 70 μL 2.5 M NaCl and 1400 μL 96% ethanol (62% final concentration) before being stored at -20 °C for at least 24 hours. The DNA was precipitated by centrifugation (25 min, 4 °C, 23 500 g, Eppendorf™ 5424R), after which it was washed once in 70% ice-cold ethanol and dried for less than 3 minutes at 37°C. The eDNA was quantified using the QuantiFluor dsDNA dye (QuantiFluor dsDNA System, Promega, Madison, WI, USA) according to the manufacturer's protocol. In brief, eDNA in each sample was mixed with 200 μL of freshly prepared QuantiFluor dsDNA dye in TE buffer and incubated for 5 minutes before measuring the fluorescence intensity. The eDNA concentration was measured in 2 μL on a (NanoDrop™ 2000, Thermo Fisher Scientific, UK), using an excitation wavelength of 504 nm and an emission wavelength of 531 nm. For each run, a calibration curve was generated using Lambda DNA (Invitrogen™ Molecular Probes). To ensure the reproducibility of the experiment, the growth and eDNA concentration were determined in three independent samples for each time point. The experiment was also repeated with triplicates for all strains to verify the reproducibility between biological replicates.

Biomass quantification

The dry matter of the liquid phase and biofilm phase were determined separately by the Moisture analyzer (HE53 Halogen Moisture Analyzer, Switzerland) according to manufacturer protocol. Briefly, the equipment was first warmed up for 30 minutes, and the standby temperature was set to 60°C. Then, the weighing aluminum pan containing a membrane filter disc (0.2μm, 47mm, Fisherbrand™) was tared automatically on the balance after being dried at 105°C in the moisture analyzer until reaching a stable weight lasting about 1 minute. The drying temperature was set to 105°C. Next, 10 mL of well-mixed planktonic and biofilm samples (After emptying the flask from planktonic culture, adherent cells were harvested by scraping from the wall of flasks with a cell scraper and resuspended in PBS and well-mixed) were evenly added to the membrane filter and positioned in a vacuum filtration apparatus. The liquid component of the sample was removed substantially by applying a vacuum from a small compressor for 2-5 minutes, leaving the broth solids. The filter and the residual solids were washed with 10 mL of deionized water, and the vacuum was reapplied to remove excess liquid. The filter and solids were replaced on an aluminum pan, and the drying program was set to end when the weight change was less than 0.1 mg min^{-1}. The loss of weight upon drying was then used to calculate biomass as grams of dry weight per liter.

Off-line flow cytometry analyses

FCM analysis was carried out with an Attune NxT Acoustic Focusing Cytometer (Thermo Fisher Scientific, United States) containing a violet laser 405 nm (50 mW), a blue laser 488 nm (50 mW), and a red laser 638 nm (100 mW). Instrument calibration was performed with Attune performance tracking beads (2.4 and 3.2 μm) (Thermo Fisher, United States). Side scatter (SSC) and Forward scatter (FSC) and BL3 (695/40) for PI (P4170, Sigma-Aldrich) were determined with FC. The software settings were as follows: Fluidics, medium; Threshold, 2000 on SSC-H; Run with limits, 40,000 events at a flow rate of 25 μl/min. Cells were diluted to an appropriate density OD600 (0.001-0.003 ≈700-1500 event/ μl) with filtered 1x PBS. FSC and SSC voltage and threshold were set based on wild-type bacteria. All bacterial samples were stained right before FC analysis by adding 1 μL of the PI stock solution (a stock solution was prepared at 1 mg mL^{-1} in sterile Milli-Q water and used at a final concentration of 1.5 μM in sterilized PBS) to 1 mL of a cell suspension in PBS (1x10^7 cells mL^{-1}). The stained samples were incubated for 10 min in the dark at room temperature and analyzed by FC (live-dead gating was done based on heat-killed bacteria at 80°C for 1 h).

Microscopy imaging

Samples from *P. putida* KT2440, *P. putida* Δ*lap*A, and *P. putida* DGC culture were taken at 0h, 6h, and 24h during the batch phase and subjected to microscopy analysis. Microscopy images were acquired using a Nikon Eclipse Ti2-E inverted automated epifluorescence microscope (Nikon Eclipse Ti2-E, Nikon France, France) equipped with a DS-Qi2 camera (Nikon camera DSQi2, Nikon, France), a 100× oil objective (CFI P-Apo DM Lambda 100× Oil (Ph3), Nikon, France).

Flow cytometry for the detection of cell aggregates

FC analysis (offline) was carried out with an Attune NxT Acoustic Focusing Cytometer (Thermo Fisher Scientific, United States). Before measurements, cell samples were diluted to 1x10^7 cells mL^{-1}. For each sample, at least 20,000 events were taken and analyzed. FC data sets were first cleaned of electronic instrument noise by eliminating events with negative, infinite, or non-numerical

values in the forward and side scattering signals. After that, all doublet events were identified and eliminated by evaluating the standardized residual value (SRV) of the expected linear ratio between the area and the height of the front scattering signal. All data sets presented less than 5% error between the electrical and doublet noise, and after data cleaning, a minimum of 20,000 events were required for further analysis. The determination and quantification of possible aggregates were done similarly to the analysis used by Velastegui.[64] In this case, a grand mean and standard deviation were calculated to propose a normal probability density function describing the cells that stay in the single non aggregated state (the vast majority) with this we constructed thresholds of increasing probability for the events to be increasing in size not conforming to a single state population but being part of another population state with different grand mean and standard deviation. Therefore, the events that fall above two standard deviations only have 5/100 probability of being part of a single cell floating population. Consequently, calculating and comparing the over-representation of this percentile across time gives us a quantitative measurement of cells that are more in not a single cell floating state. The agglomeration state was then confirmed by observations in a microscope and the final biofilm production.

Continuous cultivation with automated FC

In this study, *P. putida* KT2440 was grown in a stirred bioreactor (Biostat B-Twin, Sartorius) with a total volume of 2 L and a working volume of 1 L. The batch phase was initiated by diluting overnight cultures into a minimal medium to achieve an initial OD600 of 0.3. The culture was maintained at pH 7.2 and 30°C, with stirring set at 800 rpm and an aeration flow rate of 1 L min^{-1} (1 vvm). The depletion of oxygen marked the end of the batch phase and the start of continuous cultivation mode. For chemostat cultivations, the modified M9 medium containing 5 g L^{-1} glucose was continuously fed at a dilution rate of 0.1 h^{-1}. In contrast, for periodic pulsing system cultivations, a modified M9 medium without a carbon source was continuously fed at the same dilution rate, and glucose feed pulses (0.5 g L^{-1} per pulse) were introduced hourly. The Segregostat platform, previously described[39,65] was used as a reactive FC strategy, in which glucose was pulsed based on a predefined set point. A feedback control loop, including a custom MATLAB script based on FC data, activated a pump to pulse an actuator (glucose) accordingly. The regulation was triggered once the fluorescence threshold was exceeded by more than 10% of the PI positive cells (detected based on t he FL3-A channel). Throughout the experiments, samples were collected every 12 minutes from the bioreactor and automatically diluted and stained with PI and analyzed by flow cytometry (BD Accuri C6, BD Biosciences) based on a FSC-H threshold of 20,000.

Processing the data from automated FC and computing of the flux of cells (F) and the entropy (H) of the cell population

Microfluidics are typically used for characterizing population dynamics with a single cell resolution.[67,68] However, microfluidics cultivation experiments, as well as the associated data processing, are quite time consuming. At this level, FC can be considered as an alternative method exhibiting a higher experimental throughput,[36] but at the expense of losing the information about specific trajectories of the individual cells.[69] This drawback can be compensated by considering automated FC protocols where more regular snapshots of the population can be acquired. We used automated FC in the context of this work for tracking PI-positive, eDNA-bound, cells. Each 12 minutes, a sample was automatically taken out of the bioreactor, diluted, stained with PI and analyzed by FC. Individual snapshots can then be assembled into a time scatter plot (Figure S8A). Additional data treatment steps can also be applied for extracting information about the degree of heterogeneity of the cell population, as well as the fluxes of cells through the phenotypic space. This study employs a proxy derived from information theory i.e., information entropy H, to characterize how cell populations dispersion evolves with time.[43] Information theory is being more and more applied to study signal processing by cellular systems.[70–74] The fundamental basis of information theory relies on the quantification of information entropy (H), serving as a gauge of uncertainty regarding the cell population's response (output) concerning environmental stimuli (input).[75] However, the entropy profile H(t) will be used for characterizing the dynamics of population dispersion over time. To quantify entropy, we utilize the following equation based on the PI fluorescence distribution acquired through automated flow cytometry (FC):

$$H = -\sum_{i=1}^{m} p(x_i).\log_2 p(x_i) \qquad \text{(Equation 1)}$$

Here, m represents the number of observed states (PI classes in our case), and p denotes the probability of observing a cell displaying a specific state i.e., a given PI fluorescence intensity in our case. The probabilities for various fluorescence classes are easily determined based on automated FC. For this purpose, the PI distribution for a given interval of time is divided into 50 different bins (corresponding to m = 50 in Equation 1) and the entropy is determined based on the specific number of cells inside each bin by applying Equation 1 (Figure S8B). The number of bins has been previously shown to be optimal for determining the entropy based on FC data.[34] The binned data can also be used for determining the flux of cells (F) through the phenotypic space. For this purpose, a gradient is applied over 2 consecutive binned datasets (Figure S8C). Based on the computation, the F(t) profile can be determined. The three strains of *P. putida* were cultivated in shake flask for determining their growth in liquid culture and the switching cost related to biofilm switching (Figures S6 and S7). For this purpose, the time evolution of biomass and carbon source (glucose) were determined. Gucose concentrations were analyzed by high-performance liquid chromatography (Waters Acquity UPLC® H-Class System) using an ion exchange Aminex HPX-87H column (7.8 × 300 mm, Bio-Rad Laboratories N.V.). The analysis was carried out with an isocratic flow rate of 0.6 mL min^{-1} for 25 min at 50°C. The mobile phase was composed of an aqueous solution of 5 mM H2SO4. Elution profiles were monitored through a Waters Acquity® Refractive Index Detector (RID) (Waters, Zellik, Belgium).

Glucose standard solutions (Sigma-Aldrich, Overijse, Belgium) were used to determine the retention times and construct calibration curves.

QUANTIFICATION AND STATISTICAL ANALYSES

Automated FC data were processed with a custom-made Python toolbox (MiPI Flow Cytometry Analysis toolbox (mFCAtoolbox) – see key resources table) for determining cell aggregates and the number of PI-positive cells. For each cultivation experiments, data were generated at least in triplicates for the shake flask experiments and in duplicate for the continuous cultivation experiments. Data are presented as the mean ± standard deviation and the p-value is provided.

Data analysis was performed in Graphpad Prism version 8.0.1. Statistical differences in crystal violet assays were tested with one-way ANOVA test. Statistical differences in dry biomass in planktonic and biofilm were performed using one sample t and Wilcoxon test. Threshold for statistical significance used was $p < 0.05$. Significance is indicated in figures as follows: $p < 0.05$ *, $p < 0.01$ **, $p < 0.001$ ***, $p < 0.0001$ ****. Sample size is indicated in figure legends as n.